Available online at www.sciencedirect.com

ScienceDirect

IFAC Papers Online CONFERENCE PAPER ARCHIVE

IFAC PapersOnLine 55-6 (2022) 603–610

Advantages of flexible aircraft model based FDI ⋆,⋆⋆

Bálint Patartics * **Bálint Vanek** *

* *Institute for Computer Science and Control. H-1111 Budapest, Kende u. 13-17., Hungary (e-mails: patartics.balint@sztaki.hu, vanek@sztaki.hu)*

Abstract:
Model based Fault Detection and Isolation (FDI) in aerospace have received considerable attention and numerous algorithms are flying on-board commercial aircraft. Most of these algorithms are based on local models of aircraft components or rigid body aircraft models. On the other hand the ever more pressing requirement of performance and fuel efficiency improvement makes aircraft structures more lightweight and flexible. Actuator fault detection especially ailerons in the wing has to account for these flexible effects to provide the required performance. Within the article we show the trend how decreasing detection time necessitates the use of flexible dynamics based FDI, and show how detection and isolation performance are changing. Moreover, the article also highlights the need of robust filter synthesis methods, since a nominal H_∞ synthesis has significantly lower performance in worst-case situation than a robust μ synthesis based filter. The methods are demonstrated on a flexible aircraft demonstrator platform simulation model from the FLiPASED project.

Keywords: fault detection, flexible aircraft, robust filtering

1. INTRODUCTION

The purpose of Fault Detection and Isolation (FDI) is to develop model based tools with which anomalous behavior of dynamic systems, especially under stringent safety and reliability aspects can be captured. Aerospace is one of the premier application area of such methodology, since often it is irrational to use massive hardware redundancy and emply voting logics when the analytical redundancy within the system allows detecting faulty sensors and actuators (Goupil, 2011). Using sensor signals, flight controller commands and the model of the system, an FDI algorithm can detect faults in the actuators and sensors, e.g. loss of efficiency or runaway of a control surfaces or offset and noise in the sensor measurement. In case multiple fault detection signals are calculated the cross-coupling between so-called residuals have to be addressed as well in the isolation problem. Since the FDI solution is meant to be part of a safety system that is capable of reconfiguring other sensor and actuator resources while adopting slightly different control strategy to compensate for the detected failure as described by (Péni et al., 2018).

A popular approach to FDI is to design optimal filters that estimate the difference between the actual control surface deflection and the control command, or the actual measured quantity and the estimate of the sensor signal, calculating suitable residuals, as shown in (Chen and Patton, 2012)). One of the first application of optimal H_∞ filtering to FDI is elevator actuator and pitch rate sensor fault detection of the Boeing 747 by (Marcos et al., 2005). This article heavily depends on the work about developing an appropriate model of the aircraft (Marcos and Balas, 2004), since to use optimal filter design for FDI a suitable model of the aircraft is required. In this article and in the subsequent EU funded projects ADDSAFE and RECONFIGURE (Goupil and Marcos, 2014) several methods have been developed to improve FDI performance but all the industrial applications were tested on rigid-body aircraft models. With the rise of the Airbus A350 and the Boeing B787 airframe flexibility is becoming even more pronounced in commercial aviation. Hence, models that include flexible behaviour may be required for fault detection tasks. A flexible aircraft model is more difficult to obtain as opposed to the classical rigid body model which is usually the result of (CFD) modelling, wind tunnel testing and possibly in-flight identification. The flexible model also requires more expertise to create, is generally more complex - includes hundreds of modes vs. the 12 states in the rigid one and it is subject to more uncertainty due to the substantial increase in model parameters. The aircraft manufacturers have developed their aeroelastic modelling frameworks to construct these flexible aircraft models, what often includes finite element (FEM) modelling, aerodynamic modelling (mostly panel methods in NASTRAN) and possibly a ground vibration testing (GVT) and in-flight identification campaign (Meddaikar et al., 2019) to refine these models as opposed to the classical rigid body model development (Beard and McLain, 2012). The present paper builds on the prior results of (Patartics et al., 2021) which is one of the first article about flexible aircraft FDI along with (Ossmann and

⋆ The research leading to these results is part of the FLIPASED project. These projects have received funding from the Horizon 2020 research and innovation programme of the European Union under grant agreement No. 815058.
⋆⋆The research was supported by the Ministry of Innovation and Technology NRDI Office within the framework of the Autonomous Systems National Laboratory Program.

10.1016/j.ifacol.2022.07.194

Fig. 1. The demonstrator aircraft built for the FLIPASED project.

Pusch, 2019a) and (Liu et al., 2021). The present paper aims to provide guidelines on what detection and isolation performance can be achieved on aileron actuators, when using robust FDI filtering in the presence of uncertainty, based on rigid body and flexible aircraft modelling.

Our focus is on the unmanned demonstrator aircraft developed within the (FLEXOP, 2015) and currently used within the (FLiPASED, 2019) project, but the findings within the paper can be further generalized to flexible commercial aircraft. The demonstrator is built for flutter control experiments which was the subject of several research projects, e.g. (Ryan and Bosworth, 2014). The airframe is depicted in Fig. 1. Our goal is to detect the faults of the flutter control surfaces, what are the left and right outermost ailerons ($u_{a,L4}, u_{a,R4}$). These surfaces are coupled mostly to the flexible motion of the wings as well as to the lateral dynamics of the aircraft. Note that the aircraft is equipped with four ailerons per wing and a V-tail, hence the ruddervators affect both longitudinal and lateral motion of the aircraft. For simplicity our focus will be on the flexible and lateral dynamics, treating aileron ($u_a = u_{a,L1} = u_{a,L2} = u_{a,L3} = -u_{a,R1} = -u_{a,R2} = -u_{a,R3}$), rudder ($u_r = u_{r,LR1\&2}$), plus left ($u_{a,L4}$) and right ($u_{a,R4}$) flutter control surfaces as inputs. We will continue to refer to the control surfaces as aileron and rudder for simplicity. The block diagram of the FDI filter design problem is depicted in Fig. 2. FDI filters are designed at a range of target detection bandwidths taking the nominal model (leading to an H_∞ filtering), or taking the uncertain model (leading to μ optimal FDI problem) into consideration. The same investigation, with bandwidths ranging between realistic detection times, is repeated for the rigid and the flexible model of the aircraft. The nominal and worst-case behavior (Patartics et al., 2020) are evaluated, and a simple decision mechanism calculates the smallest detectable fault for single (left) flutter control surface; as well as the minimum fault magnitude what can be surely isolated from the other (right) flutter control surface fault. Based on these results, recommendations are made about modelling technique, sensor configuration and choice of synthesis method to use for certain performance requirements.

The rest of the paper is structured as follows. Section 2 introduces the rigid body and the flexible aircraft models, along with the used sensors and actuators. Section 3 describes how the optimal FDI filter design problem is set-up. Details of the performance evaluation with different filters along with the calculation of the smallest detectable and isolable fault is given in Section 4. Section 5 compares

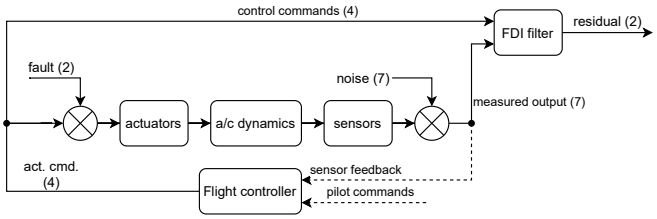

Fig. 2. Block diagram of the actuator fault detection and isolation problem.

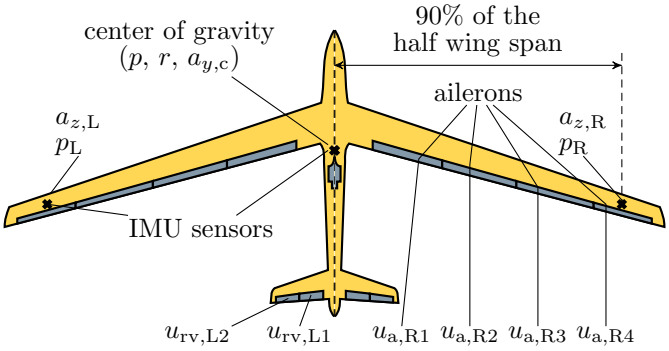

Fig. 3. Control surface configuration and sensor positions of the flexible aircraft. The control inputs and sensor signals are marked at the corresponding control surfaces and sensors.

the achieved performance of various filters designed with or without uncertainty taken into consideration, and gives recommendations on when to use a flexible aircraft model. Finally, our recommendations are summarised in Section 6.

2. RIGID AND FLEXIBLE AIRCRAFT MODELS

The demonstrator flexible aircraft, shown in Fig. 1, was built for flutter experimentation for the (FLEXOP, 2015) and subsequently for the (FLiPASED, 2019) H2020 projects. It is a high aspect ratio ($AR = 20$), single-engine aircraft, with a wingspan of 7 m, and nominal takeoff weight of 65 kg. The vehicle is equipped with large number of sensors, measuring both center-body and wing accelerations as well as angular rates, as illustrated in Fig. 3. Each wing is equipped with four ailerons, the inner three reserved for rigid body, while the outermost for flutter control purposes. Two models of this aircraft are used in this paper for FDI filter design: a low order rigid body and a higher order flexible model. Both are linear models obtained in straight and level flight (at 50 m/s), which is below the open-loop flutter speed. For FDI design purposes the longitudinal modes are removed, while lateral and asymmetric wing modal states are kept, corresponding to aileron effectiveness. Both rigid body and flexible dynamics contain the stable open-loop dynamics of the aircraft, without the baseline stability augmentation loop for simplicity. A detailed description obtaining it is discussed in (Takarics and Vanek, 2019) and (Meddaikar et al., 2019).

The outputs are sensor signals including lateral motion rigid body side acceleration (a_y), roll (p) and yaw rate (r), as well as flexible dynamics related wingtip accelerations ($a_{z,LR}$), as well as bending rates near the wingtip (p_{LR}), the 'LR' standing for Left and Right. The sensor choice is an important engineering decision and one of the key differentiator between flexible and rigid model based

FDI. The obvious decision is to use the standard IMU sensors in the c.g. as well as accelerometers in the wing - since differential acceleration between left and right side might indicate dedicated actuator movement. After fine tuning the algorithm with only these sensors ($a_{z,LR}$) the performance was not satisfactory - the minimum robustly detectable fault with flexible model was 4.1 *deg* and with the rigid model 23.5 *deg*. Hence wing angular rate sensors (available on the demonstrator) are also included in the problem. With torsion rate sensors (q_{LR}) the minimum detectable fault is 4.7*deg*, and the rigid performance improves only slightly (18.6 *deg*), introducing an artificial pitch rate sensor. In case the bending rate (p_{LR}) is the input to the filter, besides the normal accelerations, the minimum robustly detectable fault decreases to 2.4 *deg* in the flexible case and remains the same of 23.5 *deg* in the rigid case, since it is essentially equivalent to roll rate sensing at multiple locations. This led to a decision to use normal acceleration and bending rate sensors within our parametric detection and isolation performance investigation.

The sensor dynamics are assumed to be first order low pass filters of the form

$$G_{\text{sens}}(s) = \frac{1}{\frac{s}{2\pi\theta}+1}, \tag{1}$$

where θ is the bandwidth. Additive white noise disturbance is assumed on the sensor outputs. Based on the specifications of the sensors and test data with the demonstrator, the standard deviations of the sensor noises along with the bandwidths are listed in Table 1.

The four individual ruddervator tail control surfaces are linked together with a common command u_{r}, shown in Fig. 3. The aileron command considered in this paper is obtained by

$$u_{\text{a,LR1}} = 0;\ u_{\text{a,L23}} = -u_{\text{a,R23}} = u_a. \tag{2}$$

Thus, the input of the lateral dynamics system is the control command $u_{\text{c}} = [u_{\text{a}}\ u_{\text{a,L4}}\ u_{\text{a,R4}}\ u_{\text{r}}]^T$. The actuators in the wings are MKS HBL599, their dynamics are obtained with system identification:

$$G_{\text{act,a}}(s) = \frac{1817}{s^2+54.03s+1817}. \tag{3}$$

Since the four ruddervators are transformed to a single rudder, only one actuator is included in the model. The input of the unsteady aerodynamics consists of the control surface deflections, their derivatives and second derivatives, hence the derivatives of the output of $G_{\text{act,a}}(s)$ are also connected to the system.

The states of the system used for FDI design includes lateral modes: v, p, r, ϕ (side velocity, roll- and yaw-rate, roll angle), as well as 9 flexible modal states, their derivatives and 2 aerodynamic lag states, based on the model reduction framework of (Meddaikar et al., 2019), which reduces the 1152 states ASE model to 56 states, including the actuator dynamics. The rigid aircraft model is directly obtained from the reduced flexible model by residualising the flexible states (modal coordinates, their derivatives, and the lag states). In practice, a rigid model is usually the result of parameter identification or wind tunnel testing of a standard rigid model. Our approach aims to avoid any differences between the two models that do not arise from flexibility, hence the simple rigid model is derived from the flexible one.

3. FAULT DETECTION FILTER DESIGN

The FDI filter design is posed as an H_∞ optimal synthesis problem similarly to the solution of (Marcos et al., 2005), but it goes even further by handling the structured uncertainty in a systematic manner employing μ synthesis. It would be also possible to design LPV detection filters (Vanek et al., 2014) scheduled with velocity for a larger flight envelope, but the goal of this article is to highlight the need of including flexible dynamics in the design, what is already visible from a single velocity point. The generalised plant interconnection is depicted in Fig. 4. Here, $f = [f_1\ f_2]^T$ is the fault vector which is modelled as an additive disturbance on the two outermost flutter control ailerons $u_{a,LR4}$. The output of the FDI filter $F(s)$ is called the residual. It is an estimate of the fault signals hence it can be denoted by $\hat{f} = \left[\hat{f}_1\ \hat{f}_2\right]^T$. The control command u_{c} is normally the output of the flight controller but since no controller is considered in the design process, it is treated as a known external disturbance via a scaling factor W_u which normalizes the 1 norm d_u signal to the actuator limit of ± 15 *deg*.

The desired response of the residual signals to the faults is defined as

$$T_{\text{des}}(s) = \frac{1}{\kappa s+1} I_2, \tag{4}$$

where I_2 is a 2×2 identity matrix. The time constant κ is a design parameter that sets the target bandwidth (hence the speed of the response), which is part of the investigation. Fault isolation is imposed by the off-diagonal 0 terms, what ensures that f_1 will have minimal impact on r_2 and f_2 on r_1. The subsequent weight of the estimation error is also chosen to correspond to the bandwidth of $T_{\text{des}}(s)$. It is defined as

$$W_{\text{e}}(s) = \frac{0.01\kappa s+1}{\kappa s+1} I_2. \tag{5}$$

Noise cancellation is required on the frequency range beyond the bandwidth of $T_{\text{des}}(s)$. This is captured by the noise weighting function

$$W_{\text{n}}(s) = R\frac{10\sqrt{2}\kappa s+1}{\frac{\sqrt{2}\kappa}{100}s+1}, \tag{6}$$

where R is a diagonal matrix with the standard deviations of the individual noise signals in the diagonal. The weight of the input multiplicative uncertainty is

$$W_{\text{u}}(s) = \frac{(s+759)\left(s^2+26.22s+298.4\right)}{(s+680.4)(s+188.4)(s+17.66)}. \tag{7}$$

This is chosen so that the uncertain plant

$$G_{\text{plant}}(s)\left(I_4 + W_{\text{u}}(s)\,\Delta(s)\right) \tag{8}$$

has 10% uncertainty at low frequencies, 50% at the elevator actuator bandwidth, and 100% at high frequencies. Notice that $W_{\text{u}}(s)$ does not depend on κ since it describes the accuracy of the model regardless of the target bandwidth requirement. These weighting functions for $\kappa = 1\,\text{s}$ are compared in Fig. 5.

Denote the weighted design interconnection, depicted in Fig. 4, with $F(s)$ and $\Delta(s)$ left out by

Table 1. Sensor bandwidth and standard deviation of the measurement noise.

	$a_{y,c}$	p	r	$a_{z,w}$	p_w
type	MTI-G-710 xSense			MPU-9250	
bandwidth (θ)	200 Hz			200 Hz	
std. dev. of the noise	0.008 m/s^2	0.14°/s	0.14°/s	0.042 m/s^2	0.14°/s

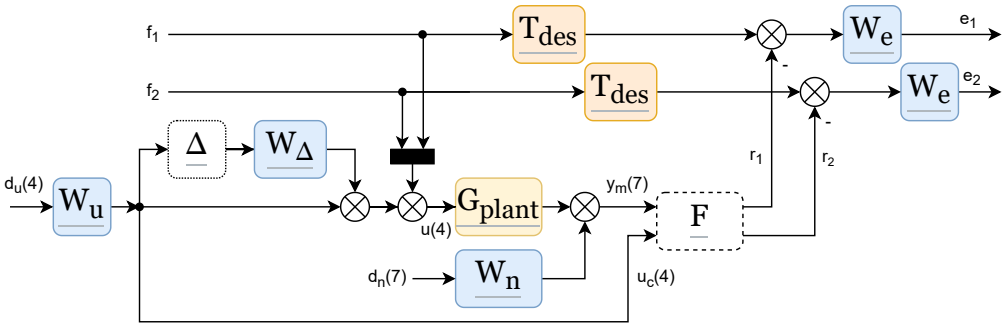

Fig. 4. Generalized plant interconnection for the H_∞ and μ FDI filter design.

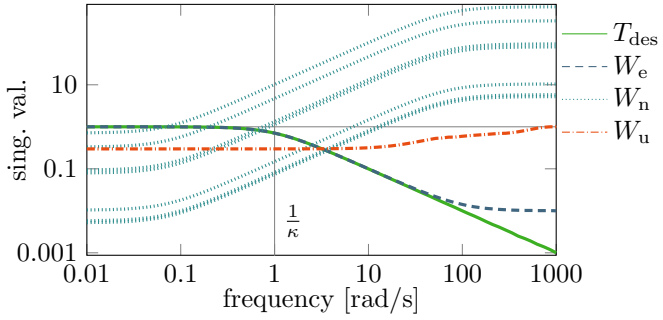

Fig. 5. Weighting functions used for the H_∞/μ synthesis. The value of the design parameter is $\kappa = 1$ s. (Since the standard deviations of the noise channels are different, $W_n(s)$ is represented by multiple lines.)

$$\begin{bmatrix} z_\Delta \\ e \\ y_m \\ u_c \end{bmatrix} = M(s) \begin{bmatrix} w_\Delta \\ f \\ d_u \\ d_n \\ r \end{bmatrix}. \tag{9}$$

To connect $\Delta(s)$ and $F(s)$, let us define the Linear Fractional Transformations (LFTs). For any two complex matrix (or dynamic system) $X = \begin{bmatrix} X_{11} & X_{12} \\ X_{21} & X_{22} \end{bmatrix}$ and Y, the upper LFT exists if X_{11} has the same size as Y^T and it is defined as

$$\mathcal{F}_U(X, Y) = X_{21} Y \left(I - X_{11} Y\right)^{-1} X_{12} + X_{22}. \tag{10}$$

Similarly, if X_{22} has the same size as Y^T, then

$$\mathcal{F}_L(X, Y) = X_{12} Y \left(I - X_{22} Y\right)^{-1} X_{21} + X_{11}. \tag{11}$$

The uncertain generalised plant is then

$$P(\Delta, s) = \mathcal{F}_U(M(s), \Delta(s)). \tag{12}$$

The objective of the design is to find a filter $F(s)$ such that the H_∞ norm of $\mathcal{F}_L(P(\Delta, s), F(s))$ is minimal for all possible uncertainties, i.e the optimisation problem is

$$\min_{F(s)} \max_{||\Delta(s)||_\infty \le 1} ||\mathcal{F}_L(P(\Delta, s), F(s))||_\infty. \tag{13}$$

Since $P(\Delta, s)$ is robustly stable (stable for all admissible $\Delta(s)$), this is equivalent to

$$\min_{F(s)} \left|\left| D \mathcal{F}_L(M(s), F(s)) D^{-1} \right|\right|_\infty. \tag{14}$$

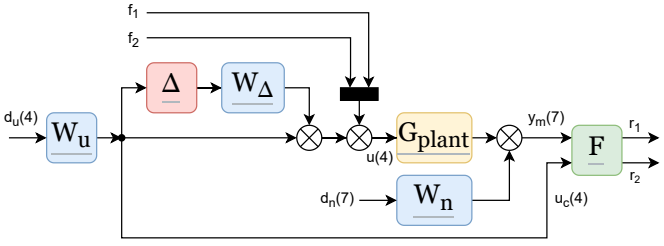

Fig. 6. Interconnection of the uncertain aircraft model and the μ or H_∞ FDI filter design used in the performance evaluation.

This optimization, without D scales is solved using the standard H_∞ synthesis tool implemented in the `hinfsyn` function of MATLAB. The version which takes uncertainty structure into consideration is an approach to minimize the upper bound for $\mu(M) \le \inf_{D \in \mathcal{D}} \bar{\sigma}(DMD^{-1})$ called D-K synthesis, implemented in the `dksyn` function of MATLAB. For details about the robust design techniques, see (Skogestad and Postlethwaite, 2007).

4. EVALUATION OF THE FAULT DETECTION PERFORMANCE

For the evaluation of the FDI filter, the weighting functions and performance output channels are removed from the generalized plant in Fig. 4. Hence, we consider the interconnection in Fig. 6. Here, $F(s)$ is the filter designed by the process described in Section 3. Let us denote the system in Fig. 6 by

$$r_{1\&2} = T(\Delta, s) \begin{bmatrix} f_{1\&2} \\ d_u \\ d_n \end{bmatrix} \tag{15}$$

For the ease of understanding, we describe the tools used to evaluate the performance of the aileron fault detection. The additional step of calculation employed for the fault isolation are also highlighted. The theoretical background of the computations involved in this section are described by (Skogestad and Postlethwaite, 2007).

The effect of the control command on the residual is measured by the worst-case gain of $T(\Delta, s)$ from the input d_u to the output $r_{1\&2}$. Denote this gain by

$$\vartheta_{\mathrm{a}} = \max_{||\Delta(s)||_\infty \leq 1} ||T_{\hat{r}_{1\&2} \leftarrow u_{\mathrm{c}}}(\Delta,\, s)\, W_u||_\infty\,, \qquad (16)$$

where $W_u = I_{4\times4}15°$ is a scaling matrix that represents the maximum control input. Details of deriving the worst-case gain for a single frequency point can be found in (Packard and Doyle, 1993), which is generalized for obtaining worst-case response at multiple selected frequency points in (Patartics et al., 2020). We use the approximation that if there is no noise and fault in the system (i.e. $n = 0$ and $f = 0$), then the residual produced by the control command alone is at most ϑ_{a} (i.e. $||r_{1\&2}||_\infty \leq \vartheta_{\mathrm{a}}$) for all admissible values of the uncertainty $\Delta(s)$. Note that strictly speaking, instead of the H_∞ norm, the induced L_∞ should be used. However, the induced L_∞ norm is difficult to compute in the presence of uncertainty. Also, these two norms bound each other up to a constant factor, therefore trends we want to observe are not influenced by the choice of the norm.

The effect of the noise on the residual is captured by the standard deviation of $r_{1\&2}$ due to the noise. This is calculated as the H_2 norm of $T(\Delta,\, s)$ from d_n to $r_{1\&2}$, i.e.

$$\sigma_{\mathrm{a}}^2 = ||T_{\hat{r}_{1\&2} \leftarrow d_n}(0,\, s)||_2\,. \qquad (17)$$

Recall that W_n is a diagonal matrix input scaling within $T_{\hat{r}_{1\&2} \leftarrow d_n}$ with the standard deviations of the noise signals on the diagonal. We use $\Delta(s) = 0$ to indicate that the value of $\Delta(s)$ is arbitrary in this computation since our model assumes no uncertainty in the system in the channels from the noise to the residual.

The above quantities are used to define the detection time and the smallest robustly detectable fault. We use a simple threshold decision logic to decide whether a fault actually occurred. In the practical implementation of an FDI system, an integration-based or an up-down counter-based decision logic is usually used as described by (Ossmann and Pusch, 2019b), and (Wheeler, 2011) respectively. A simple threshold logic approximates the behavior of those more complex solutions. The decision threshold is the maximum residual caused by the control input plus one standard deviation of the residual signal, i.e. $\vartheta_{\mathrm{a}} + \sigma_{\mathrm{a}}$.

If the residual is $\vartheta_{\mathrm{a}} + 1.3\sigma_{\mathrm{a}}$ in steady-state and without noise, then the probability that $r_{\mathrm{a}} > \vartheta_{\mathrm{a}} + \sigma_{\mathrm{a}}$ in the presence of noise is 90%. Therefore, we call the fault corresponding to this residual the smallest robustly detectable fault. It is denoted by ϕ_{a} and is defined by the equation

$$T_{r_{\mathrm{a}} \leftarrow f_{\mathrm{a}}}(0,\, 0)\, \phi_{\mathrm{a}} = \vartheta_{\mathrm{a}} + 1.3\sigma_{\mathrm{a}}. \qquad (18)$$

Note that similarly to the noise, there is no uncertainty in the channels from f to r. Therefore, the uncertainty sample $\Delta(s) = 0$ is used again in the computations. In accordance with the definition of ϕ_{a}, the detection time τ_{a} is defined as the time when the step response of $T_{r_{\mathrm{a}} \leftarrow f_{\mathrm{a}}}(0,\, s)\, \phi_{\mathrm{a}}$ crosses the threshold $\vartheta_{\mathrm{a}} + \sigma_{\mathrm{a}}$. These quantities are illustrated in Fig. 7.

The isolation decision is only slightly complicated than this. We derive the "surely" (in the worst-case sense) isolable fault using the principles described above. In our case fault a has to be distinguished from fault b. This means a size ψ_{a} fault coming from the cross channel b on the residual r_a plus the effect of noise ($1.3\sigma_{\mathrm{a}}$) and control disturbance (ϑ_{a}) should be less than the response of the minimum isolable fault ψ_{a} minus the effect of noise

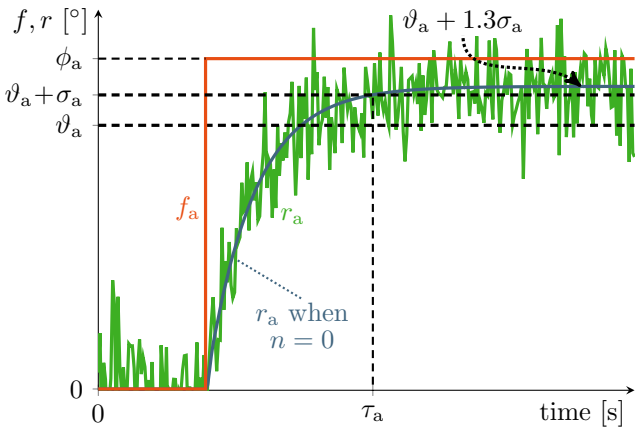

Fig. 7. Definition of the detection time and smallest detectable fault.

Table 2. Detection and isolation performance (flexible design on flexible model, $\kappa = 0.196\,\mathrm{s}$).

	H_∞ nom.	H_∞ w.c.	μ nom.	μ w.c.
Det. (°)	0.1	22.7	0.8	1.7
Isol. (°)	0.2	45.5	1.7	4.8

and control disturbance, following arguably conservative arguments, hence the description "surely".

$$\psi_{\mathrm{a}} = \frac{2(\vartheta_{\mathrm{a}} + 1.3\sigma_{\mathrm{a}})}{T_{r_{\mathrm{a}} \leftarrow f_{\mathrm{a}}}(0,\, 0) - T_{r_{\mathrm{a}} \leftarrow f_{\mathrm{b}}}(0,\, 0)}. \qquad (19)$$

For demonstration purposes, we show these performances by evaluating the filter design on the rigid aircraft model at $\kappa = 0.271$ s and on the flexible aircraft model at $\kappa = 0.196$ s. For these filter designs, we use the measurements described above, including the left and right bending rates (p_{LR}). Different time constants are chosen for the two designs, since a detailed evaluation for multiple values of κ, presented in Section 5, led to these parameter values as a compromise between detection time and minimum detectable performance. The construction of the worst-case uncertainty sample is done using the algorithms from (Patartics et al., 2020). In the present paper two distinct frequency points are chosen to realize the worst case uncertainty sample Δ - one corresponding to the classical worst-case gain, the frequency where $||T_{r_{\mathrm{a}} \leftarrow f_{\mathrm{b}}}(\Delta_{w.c.}, \omega_1) W_u||_\infty = \vartheta_{\mathrm{a}}$, and the other at $\omega_0 = 0$ to obtain the worst DC gain, which leads to the worst steady state response in time domain simulations.

When analysing the flexible design on the flexible model with $\kappa = 0.196$ s, the resulting filter bandwidths are $B_{\mathrm{a}} = 6.82$ rad/s for the μ, and $B_{\mathrm{b}} = 8.81$ rad/s for the H_∞ flexible model based filters, shown in Fig. 8. At these frequencies, the model uncertainty is still low, therefore design conditions can be met with $\mu = 0.426$ and H_∞ gain of 0.00012 for the two cases. When analyzing the filter obtained by μ synthesis designed and evaluated on the flexible aircraft model the effect of the control input to the residuals is $\vartheta_{\mathrm{nom.}} = 7.9 \times 10^{-6}°$ and $\vartheta_{\mathrm{w.c.}} = 1.3°$, in the nominal and worst-case respectively. The noise also affects the estimation of f_1 significantly, which is reflected by the value $\sigma_{\mathrm{a}} = 0.56°$. The steady state detection gain is relatively far from unity $T_{r_1 \leftarrow f_1} = 0.848$, while the cross coupling term is almost negligible $T_{r_1 \leftarrow f_2} = 0.0025$. In case of the H_∞ filter these values are slightly different, better

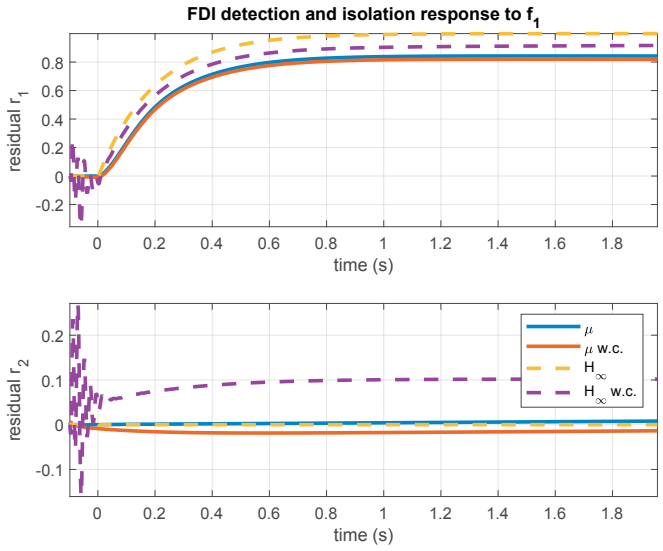

Fig. 8. FDI filter response on the *flexible* aircraft model, comparing μ and H_∞ solutions. Steady disturbance from -0.5 s, fault from 0 s.

Table 3. Detection and isolation performance (rigid design on rigid model, $\kappa = 0.271$ s).

	H_∞ nom.	H_∞ w.c.	μ nom.	μ w.c.
Det. (°)	0.4	35.6	10.0	13.6
Isol. (°)	0.8	71.5	20.8	28.4

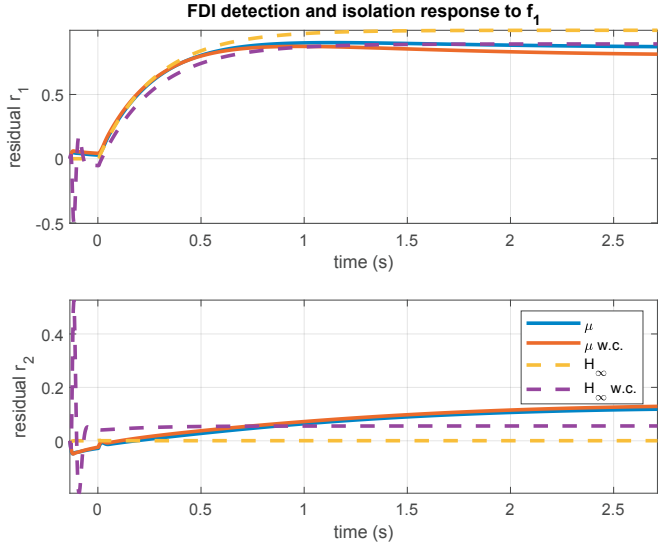

Fig. 9. FDI filter response on the *rigid* aircraft model, comparing μ and H_∞ solutions. Steady disturbance from -0.5 s, fault from 0 s.

in the nominal case and much worse in the worst-case response. The effect of the control input to the residuals is $\vartheta_{\text{nom.}} = 1.4\times10^{-6\circ}$ and $\vartheta_{\text{w.c.}} = 22.59°$, in the nominal and worst-case respectively. The noise rejection is excellent, it barely affects the estimation of $f_{1\&2}$, which is reflected by the value $\sigma_{\text{a}} = 0.074°$. The steady state detection gain is $T_{r_1\leftarrow f_1} = 0.999$, while the cross coupling term is $T_{r_1\leftarrow f_2} = 0.0035$.

In the rigid body model based synthesis, shown in Fig. 9, when $\kappa = 0.271$ s, the resulting filter bandwidths are $B_{\text{a}} = 6.26$ rad/s for the μ and $B_{\text{b}} = 6.36$ rad/s for the H_∞ filters. At these frequencies, the model uncertainty is still low, therefore design conditions can be met with $\mu = 0.475$ and H_∞=0.00035. When analyzing the filter obtained by μ synthesis on the rigid aircraft model, the effect of the control input to the residuals is $\vartheta_{\text{nom.}} = 3.7 \times 10^{-7\circ}$ and $\vartheta_{\text{w.c.}} = 3.47°$, in the nominal and worst-case respectively. The value $\vartheta_{\text{w.c.}}$ is 2.7 times higher in the rigid case than the flexible, which indicate significant performance limitations. The noise on the other hand affects the estimation of $f_{1\&2}$ more, which is reflected by the value $\sigma_{\text{a}} = 7.41°$, meaning significant sensitivity to noise when uncertainty is explicitly handled in the optimisation. The steady state detection gain is $T_{r_1\leftarrow f_1} = 0.953$, while the cross coupling term is $T_{r_1\leftarrow f_2} = 0.041$. In case of the H_∞ filter these values are slightly different, better in the nominal case and much worse in the worst-case response. The effect of the control input to the residuals is $\vartheta_{\text{nom.}} = 5\times10^{-6\circ}$ and $\vartheta_{\text{w.c.}} = 35.17°$, in the nominal and worst-case respectively. Literally meaning no fault can be detected within the actuator limits if the uncertainty is not favorable. The noise on the other hand affects the estimation of $f_{1\&2}$ much less, which is reflected by the values $\sigma_{\text{a}} = 0.33°$. The steady state detection gain is $T_{r_1\leftarrow f_1} = 1$, while the cross coupling term is $T_{r_1\leftarrow f_2} = 0.0042$. At this bandwidth, the rigid and flexible models are different, wing flexibility exhibits extra degrees of freedom, what are well captured by the wingtip acceleration and angular rates sensors. Therefore the difference between the performance measures are pronounced. The degradation is especially significant for the noise sensitivity (σ_{a}) in the consecutive (flexible vs. rigid) μ based fault estimations, and worst-case effects using the H_∞ solution also show severe degradation in $\vartheta_{\text{w.c.}}$, due to the fact that uncertainty structure is not part of the synthesis.

5. COMPARISON OF THE RIGID AND FLEXIBLE MODEL BASED DESIGNS

In this section, we compare directly the FDI filters designed for the rigid and flexible aircraft models, rigid designs are evaluated on rigid models and flexible on flexible to give a fair comparison. The performance metrics we consider are the smallest detectable fault and smallest surely isolable fault vs. the filter bandwidth as defined in Section 4. In order to study directly the effect of flexible vs. rigid model based designs all the performance weights and synthesis methods are kept the same at the corresponding κ, nominal speed of response points as described in Section 3. Our investigation revealed that besides the accelerometers placed to the wing tips, significant improvement is seen on the flexible model side when using bending rate sensors, hence this is the sensor configuration fixed for the investigation - with which the smallest fault could be detected using any sensor, model, or speed of response setting.

Figure 10. presents the trade-off between the smallest detectable fault and the detection time requirement for the actuator fault f_1 detection. Six lines, representing six cases are shown, including rigid vs. flexible cases using the filters obtained by $\mu/D-K$ synthesis. In addition the better performing, flexible model based, trends are compared to the responses with the H_∞ filter based solutions. Within each set (rigid-μ,flexible-μ,flexible-H_∞) the nominal case, with $\Delta = 0$ and the worst case sample $\Delta = \Delta_{w.c.}$ are

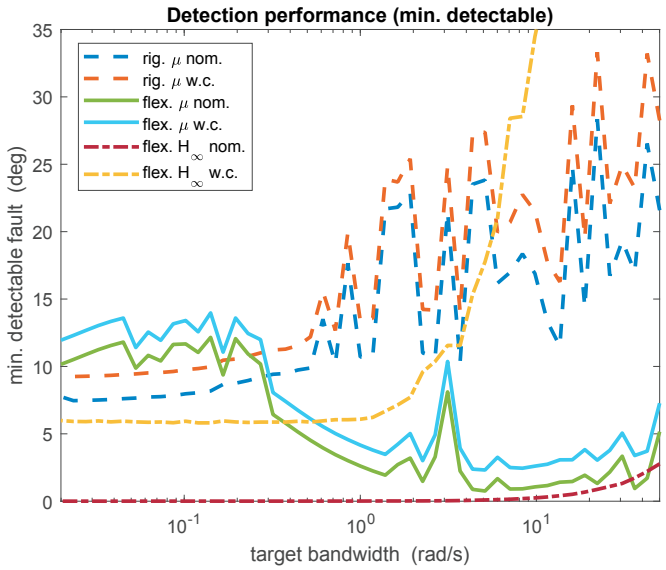

Fig. 10. Trade-off between the minimum detectable fault and the filter bandwidth for the aileron ($u_{a,L4}$) fault detection.

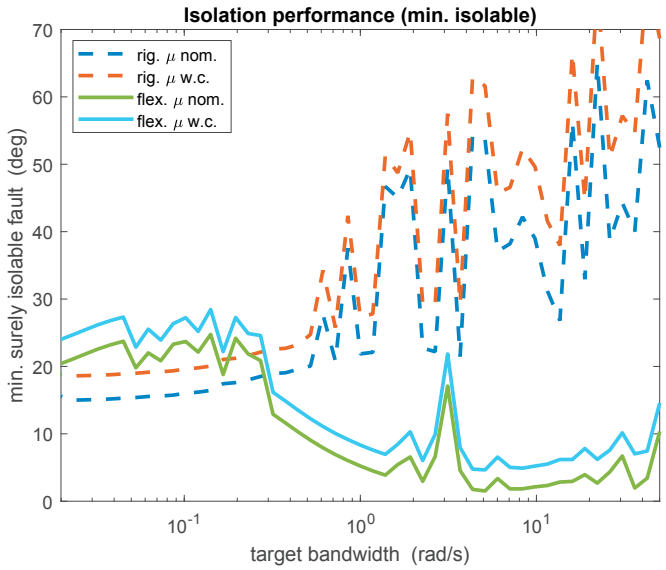

Fig. 11. Trade-off between the minimum surely isolable fault between the ailerons (isolate $u_{a,L4}$ from $u_{a,R4}$) and the filter bandwidth.

also shown. A first clear trend, that nominal values are always lower than worst-case values is clearly visible. The amount of difference is $2-4°$ in the μ synthesis case and $6-35°$ in the H_∞ case. This behavior is expected, but it is worth to mention that at low target bandwidth the H_∞ filter outperforms the μ based filters, since the problem is dominated by noise and not by uncertainty, and the H_∞ solution is able to handle that better due to fewer objectives. On the other hand as higher target bandwidth is required and the problem is more dominated by uncertainty the worst-case response with the H_∞ filter becomes unacceptable. At lower frequencies the rigid model based detection performance is slightly better than the flexible model based, but as frequency increases the detection performance degrades. On the other hand the flexible model based filter improves significantly as target bandwidth reaches 0.3 rad/s and stays there all the way till 30 rad/s, where the gap in minimum detectable fault is more than 15°. The only exception is the narrow range around 3 rad/s where the rigid-body roll mode interacts unfavorably with the flexible modes, what makes the aileron fault detection difficult at this particular frequency point.

Figure 11 presents the trade-off between the smallest surely isolable fault, defined in (19), and the target bandwidth. Four lines all corresponding to the μ-synthesis based filter designs are compared. The best performance is achieved at moderately high frequency range with the flexible model based filtering, applied to the flexible model. The rigid model based method, applied to the rigid aircraft model, even though resulting in a significantly lower state order, achieves far worst isolation performance. Taking the 15° actuator limits into account the rigid model based method is only able to isolate faults realistically if the uncertainty is smaller and not at its worst-case sample.

The trends in detection and isolation are very similar with a rough scaling factor of two, due to the fact that the cross coupling term $T_{r_1 \leftarrow f_2}(0,0)$ is almost always small compared to the direct fault to residual channel. The isolation problem, as well as the detection problem is more difficult at high frequencies with the rigid model and the best values are obtained using flexible model based design at a relatively high target bandwidth. We conclude that the performance of the aileron actuator fault detection is impacted greatly by the choice of design model, as well as the sensor configuration. It must be noted, that to perform a more realistic assessment both rigid-, and (reduced order) flexible-model based filters should be tested on the high-fidelity simulation platform of the aircraft to have a better overall picture about the real-world application of them.

6. CONCLUSIONS

Based on a specific case study, motivated by the needs of the FLiPASED demonstrator aircraft and its flutter control surfaces, guidelines are established on when it is advantageous to use flexible model based FDI filter design. It is concluded that major performance improvement is achieved in the medium to high target bandwidth range when using flexible model based filter synthesis. When considering structured uncertainty on the input channels the performance of nominal model based filters degrade rapidly as the target bandwidth increases. At the cost of loss in detection and isolation performance at the nominal point, it is more advantageous to use filter design methods capable of handling uncertainty systematically, when considering the whole range of possible uncertainties. Both the rigid and the flexible model based synthesis setups are able to achieve very small cross-coupling, when the problem solution is not influenced on the fault to residual path with uncertainty.

REFERENCES

Beard, R.W. and McLain, T.W. (2012). *Small unmanned aircraft: Theory and practice.* Princeton university press.

Chen, J. and Patton, R. (2012). *Robust Model-Based Fault Diagnosis for Dynamic Systems.* The International Series on Asian Studies in Computer and Information Science. Springer US.

FLEXOP (2015). *Flutter Free FLight Envelope eXpansion for ecOnomical Performance improvement, Horizon 2020 research and innovation programme of the European Union, grant agreement No 636307.* URL `https://flexop.eu/, Accessed on 11. 2021.`

FLiPASED (2019). *Flight Phase Adaptive Aero-Servo-Elastic Aircraft Design Methods, Horizon 2020 research and innovation programme of the European Union, grant agreement No 815058.* URL `https://flipased.eu/, Accessed on 11. 2021.`

Goupil, P. (2011). AIRBUS state of the art and practices on FDI and FTC in flight control system. *Control Engineering Practice*, 19(6), 524–539.

Goupil, P. and Marcos, A. (2014). The european addsafe project: Industrial and academic efforts towards advanced fault diagnosis. *Control Engineering Practice*, 31, 109–125.

Liu, Y., Hong, S., Zio, E., and Liu, J. (2021). Integrated fault estimation and fault-tolerant control for a flexible regional aircraft. *Chinese Journal of Aeronautics*.

Marcos, A., Ganguli, S., and Balas, G.J. (2005). An application of H_∞ fault detection and isolation to a transport aircraft. *Control Engineering Practice*, 13(1), 105–119.

Marcos, A. and Balas, G.J. (2004). Development of linear-parameter-varying models for aircraft. *Journal of Guidance, Control, and Dynamics*, 27(2), 218–228.

Meddaikar, Y.M., Dillinger, J., Klimmek, T., Krueger, W., W uestenhagen, M., Kier, T.M., Hermanutz, A., Hornung, M., Rozov, V., Breitsamter, C., et al. (2019). Aircraft aeroservoelastic modelling of the FLEXOP unmanned flying demonstrator. In *AIAA Scitech 2019 Forum*, 1815.

Ossmann, D. and Pusch, M. (2019a). Fault tolerant control of an experimental flexible wing. *Aerospace*, 6(7).

Ossmann, D. and Pusch, M. (2019b). Fault tolerant control of an experimental flexible wing. *Aerospace*, 6(7), 76.

Packard, A. and Doyle, J. (1993). The complex structured singular value. *Automatica*, 29(1), 71–109.

Patartics, B., Kumtepe, Y., Takarics, B., and Vanek, B. (2021). On the necessity of flexible modelling in fault detection for a flexible aircraft. In *2021 IFAC MECC*.

Patartics, B., Seiler, P., and Vanek, B. (2020). Construction of an uncertainty to maximize the gain at multiple frequencies. In *2020 American Control Conference (ACC)*, 2643–2648.

Péni, T., Vanek, B., Lipták, G., Szabó, Z., and Bokor, J. (2018). Nullspace-based input reconfiguration architecture for overactuated aerial vehicles. *IEEE Transactions on Control Systems Technology*, 26(5), 1826–1833.

Ryan, J.J. and Bosworth, J.T. (2014). *Current and Future Research in Active Control of Lightweight, Flexible Structures Using the X-56 Aircraft.*

Skogestad, S. and Postlethwaite, I. (2007). *Multivariable feedback control: analysis and design*, volume 2. Citeseer.

Takarics, B. and Vanek, B. (2019). Tensor product model-based robust flutter control design for the FLEXOP aircraft. *IFAC-PapersOnLine*, 52(12), 134–139. 21st IFAC Symposium on Automatic Control in Aerospace ACA 2019.

Vanek, B., Edelmayer, A., Szabó, Z., and Bokor, J. (2014). Bridging the gap between theory and practice in LPV fault detection for flight control actuators. *Control Engineering Practice*, 31, 171–182.

Wheeler, T.J. (2011). *Probabilistic performance analysis of fault diagnosis schemes.* Ph.D. thesis, UC Berkeley.